

# Dynamics of ballistic annihilation

Jarosław Piasecki<sup>1</sup>, Emmanuel Trizac<sup>2</sup> and Michel Droz<sup>3</sup>

<sup>1</sup> *Institute of Theoretical Physics, University of Warsaw, Hoza 69, 00-681 Warsaw, Poland*

<sup>2</sup> *Laboratoire de Physique Théorique\*, Bâtiment 210, Université de Paris-Sud, 91405 Orsay, France*

<sup>3</sup> *Département de Physique, Université de Genève, CH-1211 Genève 4, Switzerland*

The problem of ballistically controlled annihilation is revisited for general initial velocity distributions and arbitrary dimension. An analytical derivation of the hierarchy equations obeyed by the reduced distributions is given, and a scaling analysis of the corresponding spatially homogeneous system is performed. This approach points to the relevance of the non-linear Boltzmann equation for dimensions larger than one and provides expressions for the exponents describing the decay of the particle density  $n(t) \propto t^{-\xi}$  and the root mean-square velocity  $\bar{v} \propto t^{-\gamma}$  in term of a parameter related to the dissipation of kinetic energy. The Boltzmann equation is then solved perturbatively within a systematic expansion in Sonine polynomials. Analytical expressions for the exponents  $\xi$  and  $\gamma$  are obtained in arbitrary dimension as a function of the parameter  $\mu$  characterizing the small velocity behavior of the initial velocity distribution. Moreover, the leading non-Gaussian corrections to the scaled velocity distribution are computed. These expressions for the scaling exponents are in good agreement with the values reported in the literature for continuous velocity distributions in  $d = 1$ . For the two dimensional case, we implement Monte-Carlo and molecular dynamics simulations that turn out to be in excellent agreement with the analytical predictions.

## I. INTRODUCTION

Ballistically controlled reactions provide simple examples of non-equilibrium systems with complex kinetics. They consist of an assembly of particles with a given velocity distribution, moving freely between collisions in a  $d$ -dimensional space. In the simplest version of these models we consider here, when two particles meet, they instantaneously annihilate each other and disappear from the system. Despite its apparent simplicity, this problem is highly non trivial and has attracted substantial interest during the past years [1, 2, 3, 4, 5, 6, 7, 8, 9, 10]. The one-dimensional case where the particles can only have two velocities  $\pm c$  has been studied in a pioneering work by Elskens and Frisch [1]. In particular, they proved that for a symmetric initial velocity distribution, the particle density is decreasing, in the long time limit, as  $n(t) \propto t^{-\xi} \propto t^{-1/2}$ . The case of general distributions in dimension  $d = 1$  was discussed by Piasecki [2], who reduced exactly the annihilation dynamics to a single closed equation for the two-particle conditional probability. Moreover, it was shown in the particular bimodal situation of a discrete velocity distribution ( $\pm c$ ) that in one dimension, important dynamical correlations are developing during the time evolution, invalidating mean-field or Boltzmann-like approaches. This exact approach was applied to the case of a three velocity distribution by Droz et al [3], with the result that the dynamical exponents were strongly depending upon the details of the initial velocity distribution.

No analytical solutions could be found for continuous velocity distributions. In one dimension, Ben-Naim et al.[4, 5] have shown that the exponent  $\xi$  could depend on the behavior near the origin of the initial velocity distribution. This problem has been revisited by Rey et al [6]. Based on the exact theoretical approach [2, 3], a dynamical scaling theory was derived and its validity supported by numerical simulations for several velocity distributions. This leads to the conjecture that all continuous velocity distributions  $f(v)$  that are symmetric, regular, and such that  $f(0) \neq 0$  are attracted, in the long-time regime, towards the same distribution and thus belong to the same universality class. This conjecture was reinforced by numerical simulations in two dimensions [10].

The case of a continuous velocity distribution has also been approached recently by Krapivsky and Sire [9]. Starting from a Boltzmann equation, they investigated the decay of the particle density  $n(t) \sim t^{-\xi}$  and the root mean-square velocity  $\bar{v} \propto t^{-\gamma}$ . They derived upper and lower bounds for the exponents as well as their leading expansion in  $1/d$ , valid in high dimension. The main question with such an approach concerns the validity of a Boltzmann equation. This is not justified in 1D and remains an open problem in higher dimensions.

The purpose of this paper is to give a first principle answer to this type of question. The article is organized as follows. In section II, an original analytical derivation of the equations governing the dynamics of ballistic annihilation is given. The hierarchy equations obeyed by the reduced distributions are obtained. It is shown that in the Grad limit, the hierarchy formally reduces to a Boltzmann-like form for  $d > 1$ . If the initial reduced distributions factorize, the whole hierarchy reduces to one non-linear equation. In the second part of section II, a scaling analysis of the

---

\* Unité Mixte de Recherche 8627 du CNRS

exact spatially homogeneous hierarchy is performed. The exponents  $\xi$  and  $\gamma$  are showed to depend only on one parameter  $\alpha$  related to the dissipation of energy. This scaling analysis turns out to be invalid for the case  $d = 1$  with discrete velocity distributions, but correct in the continuous case. Strong arguments are given in favor of the validity of the Boltzmann approach for the case  $d > 1$  in the long time limit. The Boltzmann equation is then solved within a systematic approximation based on an expansion in Sonine polynomials (section III). The first non-Gaussian corrections to the scaled velocity distribution are computed and predictions for the exponents  $\xi$  and  $\gamma$  are explicitly worked out as a function of the dimension  $d$  and the parameter  $\mu$  characterizing the small velocity behaviour of the initial velocity distribution:  $[f(\mathbf{v}, t = 0) \propto |\mathbf{v}|^\mu \text{ for } |\mathbf{v}| \rightarrow 0]$ . These predictions for  $\xi$  and  $\gamma$  are asymptotically exact for large dimensions, and reproduce the  $1/d$  correction to the mean-field values. In 1D, they are in very good agreement with the exponents reported in the literature [9] at the Boltzmann level. In 2D, we implement extensive Direct Simulation Monte Carlo methods (DSMC) where the non-linear Boltzmann equation is solved, and Molecular Dynamics (MD) simulations where the exact equations of motion are integrated (section IV). The agreement between the MD and DSMC routes confirms the validity of the Boltzmann approach, and the decay exponents measured are in exceptionally good agreement with the Sonine prediction. Conclusions are drawn in section V. A preliminary account of part of the results presented here has been published elsewhere [10].

## II. EXACT RESULTS

### A. Derivation of the hierarchy

Let  $\Omega$  be a region of finite measure in  $R^{2d}$ . We denote by

$$\mu_k^\Omega(\mathbf{r}_1, \mathbf{v}_1, \dots, \mathbf{r}_k, \mathbf{v}_k; t) \quad (1)$$

the probability density for finding at time  $t$  exactly  $k$  particles within  $\Omega$  in the states  $(\mathbf{r}_j, \mathbf{v}_j) \in \Omega$ ,  $j = 1, 2, \dots, k$ , where  $\mathbf{r}_j$  and  $\mathbf{v}_j$  are the position and the velocity vectors, respectively. The knowledge of the densities  $\mu_k^\Omega$  for all  $\Omega \in R^{2d}$  and  $k = 0, 1, 2, \dots$ , defines entirely the state of the system. For a given region  $\Omega$  the normalization condition reads

$$\mu_0^\Omega(t) + \sum_{k=1}^{\infty} \int_{\Omega} d\mathbf{r}_1 d\mathbf{v}_1 \dots \int_{\Omega} d\mathbf{r}_k d\mathbf{v}_k \mu_k^\Omega(\mathbf{r}_1, \mathbf{v}_1, \dots, \mathbf{r}_k, \mathbf{v}_k; t) = 1 \quad (2)$$

where  $\mu_0^\Omega(t)$  is the probability of finding the region  $\Omega$  void of particles at time  $t$ .

A necessary condition for the occurrence of a pair of particles at the phase space points  $(\mathbf{r}_j, \mathbf{v}_j)$ ,  $(\mathbf{r}_i, \mathbf{v}_i)$  at time  $t > 0$  is that  $\mathbf{r}_{ij} = \mathbf{r}_i - \mathbf{r}_j$ ,  $\mathbf{v}_{ij} = \mathbf{v}_i - \mathbf{v}_j$  belong to the region of the phase space with the characteristic function

$$\begin{aligned} \chi(\mathbf{r}_{ij}, \mathbf{v}_{ij}; t) = & \theta(|\mathbf{r}_{ij}| - \sigma) \left\{ 1 - \theta(\mathbf{r}_{ij} \cdot \mathbf{v}_{ij}) \theta \left( \sigma - \sqrt{|\mathbf{r}_{ij}|^2 - (\mathbf{r}_{ij} \cdot \hat{\mathbf{v}}_{ij})^2} \right) \right. \\ & \left. \times \theta \left( |\mathbf{v}_{ij}|t - \mathbf{r}_{ij} \cdot \hat{\mathbf{v}}_{ij} + \sqrt{\sigma^2 - |\mathbf{r}_{ij}|^2 + (\mathbf{r}_{ij} \cdot \hat{\mathbf{v}}_{ij})^2} \right) \right\} \end{aligned} \quad (3)$$

where  $\sigma$  denotes the particle diameter,  $\hat{\mathbf{v}}_{ij}$  is a unit vector in the direction of the relative velocity, and  $\theta$  denotes the Heaviside distribution. Indeed, moving backward in time the particles collide during the time interval  $(0, t)$  if and only if the following three conditions are simultaneously satisfied

- |       |  |  |
|-------|--|--|
| (i)   | $\mathbf{r}_{ij} \cdot \mathbf{v}_{ij} > 0$  | particles approach each other  |
| (ii)  | $\sigma > \sqrt{ \mathbf{r}_{ij} ^2 - (\mathbf{r}_{ij} \cdot \hat{\mathbf{v}}_{ij})^2}$  | the impact parameter is smaller than $\sigma$                          |
| (iii) | $ \mathbf{v}_{ij} t > \mathbf{r}_{ij} \cdot \hat{\mathbf{v}}_{ij} - \sqrt{\sigma^2 -  \mathbf{r}_{ij} ^2 + (\mathbf{r}_{ij} \cdot \hat{\mathbf{v}}_{ij})^2}$ | the time $t$ is long enough for the overlapping configuration to occur |

Hence,  $\chi(\mathbf{r}_{ij}, \mathbf{v}_{ij}; t) = 1$ , if and only if no overlapping takes place during the time interval  $(0, t)$ .

At time  $t$  particles  $1, 2, \dots, k$  occupy in  $\Omega$  the one-particles states

$$(\mathbf{r}_1, \mathbf{v}_1), (\mathbf{r}_2, \mathbf{v}_2) \dots (\mathbf{r}_k, \mathbf{v}_k) \quad (4)$$

with probability density (1). Using the characteristic function (3) we can construct the probability density for finding the same particles in the phase space configuration

$$(\mathbf{r}_1 + \mathbf{v}_1 dt, \mathbf{v}_1), (\mathbf{r}_2 + \mathbf{v}_2 dt, \mathbf{v}_2) \dots (\mathbf{r}_k + \mathbf{v}_k dt, \mathbf{v}_k) \quad (5)$$

at time  $(t + dt)$ ,  $dt > 0$ . It reads

$$\left[ \prod_{i < j}^k \chi(\mathbf{r}_{ij} + \mathbf{v}_{ij} dt, \mathbf{v}_{ij}; t + dt) \right] \mu_k^\Omega(\mathbf{r}_1, \mathbf{v}_1, \dots, \mathbf{r}_k, \mathbf{v}_k; t) \quad (6)$$

In the limit  $dt \rightarrow 0^+$  the above expression takes the asymptotic form

$$\mu_k^\Omega(\mathbf{r}_1, \mathbf{v}_1, \dots, \mathbf{r}_k, \mathbf{v}_k; t) \left[ 1 + \sum_{i < j}^k \sum_j^k \left( \frac{\partial}{\partial t} + \mathbf{v}_{ij} \cdot \frac{\partial}{\partial \mathbf{r}_{ij}} \right) \chi(\mathbf{r}_{ij}, \mathbf{v}_{ij}; t) dt \right] \quad (7)$$

Using the definition (3) we find

$$\left( \frac{\partial}{\partial t} + \mathbf{v}_{ij} \cdot \frac{\partial}{\partial \mathbf{r}_{ij}} \right) \chi(\mathbf{r}_{ij}, \mathbf{v}_{ij}; t) = (\hat{\mathbf{r}}_{ij} \cdot \mathbf{v}_{ij}) \delta(|\mathbf{r}_{ij}| - \sigma) [1 - \theta(\mathbf{r}_{ij} \cdot \mathbf{v}_{ij})] \quad (8)$$

where  $\hat{\mathbf{r}}_{ij} = \mathbf{r}_{ij}/|\mathbf{r}_{ij}|$ . We denote by  $T^v(i, j)$  the right hand side of (8) and rewrite it in the form

$$T^v(i, j) = \sigma^{d-1} \int d\hat{\boldsymbol{\sigma}} (\hat{\boldsymbol{\sigma}} \cdot \mathbf{v}_{ij}) \theta(-\hat{\boldsymbol{\sigma}} \cdot \mathbf{v}_{ij}) \delta(\mathbf{r}_{ij} - \sigma \hat{\boldsymbol{\sigma}}) \quad (9)$$

Here  $\hat{\boldsymbol{\sigma}}$  is the unit vector along the line passing through the centers of the spheres at contact. The integration with respect to the measure  $d\hat{\boldsymbol{\sigma}}$  is thus the angular integration over the solid angle in  $d$ -dimensional space. The  $\theta$  function in (9) restricts this angular integral to the hemisphere corresponding to pre-collisional configurations.

Our aim is to construct the probability density  $\mu_k^\Omega$  at time  $(t + dt)$  for  $dt \rightarrow 0^+$  :

$$\mu_k^\Omega(\mathbf{r}_1 + \mathbf{v}_1 dt, \mathbf{v}_1, \dots, \mathbf{r}_k + \mathbf{v}_k dt, \mathbf{v}_k; t + dt) = \mu_k^\Omega(\mathbf{r}_1, \mathbf{v}_1, \dots, \mathbf{r}_k, \mathbf{v}_k; t) \quad (10)$$

$$+ \left( \frac{\partial}{\partial t} + \sum_{j=1}^k \mathbf{v}_j \cdot \frac{\partial}{\partial \mathbf{r}_j} \right) \mu_k^\Omega(\mathbf{r}_1, \mathbf{v}_1, \dots, \mathbf{r}_k, \mathbf{v}_k; t) dt$$

To this end we have still to add to the term (7) the probability weights of two events. The first corresponds to the presence at time  $t$  of  $(k + 2)$  particles within  $\Omega$  in the states

$$(\mathbf{r}_1, \mathbf{v}_1), (\mathbf{r}_2, \mathbf{v}_2), \dots, (\mathbf{r}_k, \mathbf{v}_k), (\mathbf{r}_{k+1}, \mathbf{v}_{k+1}), (\mathbf{r}_{k+2}, \mathbf{v}_{k+2}) \quad (11)$$

The state (11) is then transformed into (4) at time  $(t + dt)$  as the result of an annihilating collision between the particles  $(k + 1)$  and  $(k + 2)$ , during the time interval  $(t, t + dt)$ . According to equations (7) and (8), the rate of the occurrence of binary collisions between pairs  $(i, j)$  is obtained by applying the operator  $[-T^v(i, j)]$  defined in (9) to the corresponding distribution. Hence, when  $dt \rightarrow 0^+$ , the  $(k + 1, k + 2)$  annihilation process contributes to the density (10) the term

$$- \int_{\Omega} d(k + 1) \int_{\Omega} d(k + 2) T^v(k + 1, k + 2) \mu_{k+2}^\Omega(1, 2, \dots, k, k + 1, k + 2; t) dt \quad (12)$$

where the shorthand notation  $dj \equiv d\mathbf{r}_j d\mathbf{v}_j$  for  $j = 1, 2, \dots$  has been used.

Finally, we have to take into account the effects of the free flow of particles across the boundary  $\partial\Omega$  of the region  $\Omega$ . Indeed, the  $k$ -particle state can be created or destroyed by an additional particle  $(k + 1)$  leaving or entering the considered region. Denoting by  $\hat{\mathbf{n}}$  the unit vector normal to  $\partial\Omega$  oriented outwards, we get the term

$$\begin{aligned} & \int d\mathbf{v}_{k+1} \int_{\partial\Omega} dS (\hat{\mathbf{n}} \cdot \mathbf{v}_{k+1}) \mu_{k+1}^\Omega(1, \dots, k, k + 1; t) dt \\ &= \int_{\Omega} d(k + 1) \mathbf{v}_{k+1} \cdot \frac{\partial}{\partial \mathbf{r}_{k+1}} \mu_{k+1}^\Omega(1, \dots, k, k + 1; t) dt \end{aligned} \quad (13)$$

Here  $dS$  is the measure of the surface area, and the equality (13) follows from Gauss' theorem.

The enumerated events combine together to create the complete rate of change of the probability density  $\mu_k^\Omega$ . As equivalent events have the same probability measure we can equate (10) with the sum of contributions (7),(12) and (13) obtaining thus the hierarchy equations ( $k = 1, 2, \dots$ )

$$\left( \frac{\partial}{\partial t} + \sum_{j=1}^k \mathbf{v}_j \cdot \frac{\partial}{\partial \mathbf{r}_j} - \sum_{i < j}^k \sum_j^k T^v(i, j) \right) \mu_k^\Omega(1, \dots, k; t) =$$

$$- \int_{\Omega} d(k+1) \int_{\Omega} d(k+2) T^v(k+1, k+2) \mu_{k+2}^\Omega(1, 2, \dots, k+2; t) + \int_{\Omega} d(k+1) \mathbf{v}_{k+1} \cdot \frac{\partial}{\partial \mathbf{r}_{k+1}} \mu_{k+1}^\Omega(1, \dots, k, k+1; t).$$

Finally, the evolution equation for  $\mu_0^\Omega$  follows from the normalization condition (2). This completes the derivation of the infinite hierarchy of equations satisfied by the probability densities  $\mu_k^\Omega$ .

From (14) one can derive in a straightforward way the hierarchy satisfied by the reduced distributions  $f_k(1, 2, \dots, k; t)$ . They are relevant for the evaluation of physical parameters, as  $f_k(1, 2, \dots, k; t) d1 \dots dk$  represents the measure of the number of  $k$ -particle phase space configurations, with  $k$  particles occupying the one-particle states  $(\mathbf{r}_1, \mathbf{v}_1), (\mathbf{r}_2, \mathbf{v}_2) \dots (\mathbf{r}_k, \mathbf{v}_k)$  at time  $t$ . The distributions  $f_k$  are related to the probability densities  $\mu_k^\Omega$  by the equation [11]

$$f_k(1, 2, \dots, k; t) = \sum_{p=0}^{\infty} \frac{(k+p)!}{p!} \int_{\Omega} d(k+1) \dots \int_{\Omega} d(k+p) \mu_{k+p}^\Omega(1, \dots, k, k+1, \dots, k+p; t). \quad (15)$$

Note that the  $f_k(1, 2, \dots, k; t)$  do not depend on  $\Omega$ .

In order to derive the evolution equation for  $f_k$  one has thus to consider the hierarchy equation (14) with  $k$  replaced by  $(k+p)$ , and use the relation (15). One finds

$$\left( \frac{\partial}{\partial t} + \sum_{j=1}^k \mathbf{v}_j \cdot \frac{\partial}{\partial \mathbf{r}_j} - \sum_{i < j}^k \sum_j^k T^v(i, j) \right) f_k(1, \dots, k; t) = \sum_{p=0}^{\infty} \frac{(k+p)!}{p!} \int_{\Omega} d(k+1) \dots \int_{\Omega} d(k+p)$$

$$\left\{ \left[ - \sum_{j=k+1}^{k+p} \mathbf{v}_j \cdot \frac{\partial}{\partial \mathbf{r}_j} + \sum_{j=1}^k \sum_{i=k+1}^{k+p} T^v(i, j) + \sum_{k+1 \leq i < j}^{k+p} T^v(i, j) \right] \mu_{k+p}^\Omega(1, \dots, k+p; t) \right.$$

$$- \int_{\Omega} d(k+p+1) \int_{\Omega} d(k+p+2) T^v(k+p+1, k+p+2) \mu_{k+p+2}^\Omega(1, \dots, k+p+1, k+p+2; t)$$

$$\left. + \int_{\Omega} d(k+p+1) \left( \mathbf{v}_{k+p+1} \cdot \frac{\partial}{\partial \mathbf{r}_{k+p+1}} \right) \mu_{k+p+1}^\Omega(1, \dots, k+p+1; t) \right\}$$

It is then a question of inspection to see that on the right hand side of (16) only the term

$$\sum_{p=1}^{\infty} \frac{(k+p)!}{p!} \int_{\Omega} d(k+1) \dots \int_{\Omega} d(k+p) \sum_{j=1}^k \sum_{i=k+1}^{k+p} T^v(i, j) \mu_{k+p}^\Omega(1, \dots, k+p; t)$$

$$= \int_{\Omega} d(k+1) \sum_{j=1}^k T^v(j, k+1) f_{k+1}(1, \dots, k, k+1; t)$$

survives. All the remaining terms exactly cancel out.

The hierarchy equations satisfied by the reduced distributions  $f_k$  describing the annihilation dynamics thus read

$$\left( \frac{\partial}{\partial t} + \sum_{j=1}^k \mathbf{v}_j \cdot \frac{\partial}{\partial \mathbf{r}_j} - \sum_{i < j}^k \sum_j^k T^v(i, j) \right) f_k(1, \dots, k; t) = \int_{\Omega} d(k+1) \sum_{j=1}^k T^v(j, k+1) f_{k+1}(1, \dots, k, k+1; t). \quad (18)$$

Consider now equations (18) supposing that the state of the system is spatially homogeneous. In this case the distribution  $f_1$  does not depend on the particle position. Let us formally take the Grad limit

$$\sigma \rightarrow 0, \quad n(t) \rightarrow \infty, \quad n(t)\sigma^{d-1} = \lambda^{-1} = \text{const} \quad (19)$$

where

$$n(t) = \int d\mathbf{v} f_1(\mathbf{v}; t)$$

The fixed mean free path  $\lambda$  introduces a relevant length scale, so we pass to dimensionless positions putting

$$\mathbf{r}_j = \lambda \mathbf{x}_j, \quad j = 1, 2, \dots \quad (20)$$

With this change of variables the collision operator (9) takes the form

$$T^v(i, j) = [n(t)\sigma^d]^{d-1} \frac{1}{\lambda} \int d\hat{\sigma} (\hat{\sigma} \cdot \mathbf{v}_{ij}) \theta(-\hat{\sigma} \cdot \mathbf{v}_{ij}) \delta[\mathbf{x}_{ij} - n(t)\sigma^d \hat{\sigma}] \quad (21)$$

We conclude that the term on the left hand side of equation (18) involving the collision operators (21) vanishes in the Grad limit for  $d > 1$ , because the dimensionless parameter  $n(t)\sigma^d$  tends to zero. Note that this term induces dynamical correlations, hindering the propagation of the molecular chaos factorization. On the other hand, using the definition of  $T^v(j, k+1)$  we find that the term on the right hand side equals

$$\frac{1}{\lambda} \sum_{j=1}^k \int d\mathbf{v}_{k+1} \int d\hat{\sigma} (\hat{\sigma} \cdot \mathbf{v}_{j(k+1)}) \theta(-\hat{\sigma} \cdot \mathbf{v}_{j(k+1)}) f_{k+1}(1, \dots, j, \dots, k, \mathbf{r}_{k+1} = \mathbf{r}_j - \sigma \hat{\sigma}, \mathbf{v}_{k+1}; t) / n(t) \quad (22)$$

and its prefactor  $1/\lambda$  remains finite in the same limit. So, formally the hierarchy equations (18) at a given time  $t$  reduce pointwise in the Grad limit to the Boltzmann-like hierarchy

$$\left( \frac{\partial}{\partial t} + \sum_{j=1}^k \mathbf{v}_j \cdot \frac{\partial}{\partial \mathbf{r}_j} \right) f_k^B(1, \dots, k; t) = \int d(k+1) \sum_{j=1}^k T^v(j, k+1) f_{k+1}^B(1, \dots, k, k+1; t), \quad (k = 1, 2, \dots) \quad (23)$$

The hierarchy (23) propagates the factorization of the reduced distributions

$$f_k^B(1, \dots, k; t) = \prod_{j=1}^k f_j^B(j; t) \quad (24)$$

Hence, if the initial state is factorized, the whole hierarchy (23) reduces to one non-linear equation

$$\left( \frac{\partial}{\partial t} + \mathbf{v}_1 \cdot \frac{\partial}{\partial \mathbf{r}_1} \right) f^B(1; t) = \int d2 T^v(1, 2) f^B(1; t) f^B(2; t) \quad (25)$$

Equation (25) is the Boltzmann kinetic equation corresponding to the annihilation dynamics. In the following section, we shall see that the formal Grad limit taken here, where  $n \rightarrow \infty$ , is relevant for the description of the annihilation dynamics at late times, even if the density  $n(t)$  decreases with time.

## B. Scaling analysis of the hierarchy

The evolution of the annihilation kinetics shares a common feature with the Grad limit: The ratio of particle diameter to mean-free-path  $\lambda = 1/(n\sigma^{d-1})$ , which is related to the packing fraction, vanishes in both cases. To be more specific, we perform a scaling analysis of the exact *homogeneous* hierarchy equations and look for self-similar reduced distributions where the time dependence has been absorbed into the density  $n(t)$ , with the velocities  $\mathbf{v}$  and positions  $\mathbf{r}$  renormalized by the typical (root mean squared) velocity  $\bar{v}(t)$  and mean-free-path respectively: We define the reduced variables

$$\mathbf{c} = \frac{\mathbf{v}}{\bar{v}} \quad \text{and} \quad \mathbf{x} = \frac{\mathbf{r}}{\lambda}, \quad \text{with} \quad (\bar{v})^2 = \frac{1}{n(t)} \int v^2 f_1(\mathbf{v}; t) d\mathbf{v}. \quad (26)$$

For the one-body distribution, we therefore introduce the reduced function  $\tilde{f}_1$  such that

$$f_1(\mathbf{v}; t) = \frac{n(t)}{\bar{v}(t)^d} \tilde{f}_1(\mathbf{c}) = \frac{n(t)}{\bar{v}(t)^d} \tilde{f}_1\left(\frac{\mathbf{v}}{\bar{v}(t)}\right). \quad (27)$$

By definition, the moments of order 0 and 2 of  $\tilde{f}_1$  are constrained to unity. Requiring that the  $k$ -body distribution  $f_k$  factorizes into  $\prod_{i=1}^k f_1(i)$  in the limit of infinite relative separations between the particles, we consistently obtain the scaling form:

$$f_k(\mathbf{r}_1, \mathbf{v}_1, \dots, \mathbf{r}_k, \mathbf{v}_k; t) = \left(\frac{n}{\bar{v}^d}\right)^k \tilde{f}_k(\mathbf{x}_1, \mathbf{c}_1, \dots, \mathbf{x}_k, \mathbf{c}_k). \quad (28)$$

The evolution equations of  $n(t)$  and kinetic energy density  $n\bar{v}^2(t)$  follow from integrating (18) with weights  $d\mathbf{v}_1$  and  $v_1^2 d\mathbf{v}_1$  respectively, for  $k = 1$ . We obtain

$$\frac{dn}{dt} = -\omega(t) n \quad (29)$$

$$\frac{d(n\bar{v}^2)}{dt} = -\alpha \omega(t) n \bar{v}^2, \quad (30)$$

where the collision frequency  $\omega$  and kinetic energy dissipation parameter  $\alpha$  read

$$\omega(t) = n(t)\bar{v}(t) \int d\mathbf{c}_1 d\mathbf{c}_2 d\hat{\boldsymbol{\sigma}} (-\hat{\boldsymbol{\sigma}} \cdot \mathbf{c}_{12}) \theta(-\hat{\boldsymbol{\sigma}} \cdot \mathbf{c}_{12}) \tilde{f}_2(\mathbf{c}_1, \mathbf{c}_2, \sigma \hat{\boldsymbol{\sigma}}) \quad (31)$$

$$\alpha = \frac{\int d\mathbf{c}_1 d\mathbf{c}_2 d\hat{\boldsymbol{\sigma}} (\hat{\boldsymbol{\sigma}} \cdot \mathbf{c}_{12}) \theta(-\hat{\boldsymbol{\sigma}} \cdot \mathbf{c}_{12}) c_1^2 \tilde{f}_2(\mathbf{c}_1, \mathbf{c}_2, \sigma \hat{\boldsymbol{\sigma}})}{\left[ \int c^2 \tilde{f}_1(\mathbf{c}) d\mathbf{c} \right] \left[ \int d\mathbf{c}_1 d\mathbf{c}_2 d\hat{\boldsymbol{\sigma}} (\hat{\boldsymbol{\sigma}} \cdot \mathbf{c}_{12}) \theta(-\hat{\boldsymbol{\sigma}} \cdot \mathbf{c}_{12}) \tilde{f}_2(\mathbf{c}_1, \mathbf{c}_2, \sigma \hat{\boldsymbol{\sigma}}) \right]}. \quad (32)$$

Equation (32) is valid for general velocity rescalings; The definition (26) chosen here implies that the term  $\int c^2 \tilde{f}_1(\mathbf{c}) d\mathbf{c}$  in the denominator equals unity. The coefficient  $\alpha$  may be seen as the ratio of the kinetic energy dissipated in a typical collision normalized by the average kinetic energy, and is time-independent in the scaling regime. It is convenient to introduce the internal “clock”  $\mathcal{C}$  of the dynamics counting the number of collisions, such that  $d\mathcal{C} = \omega dt$ . With this variable, Eqs. (29) and (30) integrate into

$$n(t) = n_0 \exp[-\mathcal{C}(t)] \quad \text{and} \quad \bar{v}^2(t) = \bar{v}_0^2 \exp[-(\alpha - 1)\mathcal{C}(t)], \quad (33)$$

where the time origin with density  $n_0$  and kinetic energy density  $n_0 \bar{v}_0^2$  has been chosen to coincide with  $\mathcal{C} = 0$ . Knowledge of the  $\mathcal{C}$ -dependence of  $n$  and  $\bar{v}$  allows to relate absolute time  $t$  to the number of accumulated collisions: From Eq. (31), we have

$$\frac{d\mathcal{C}}{dt} = \omega_0 \frac{n}{n_0} \frac{\bar{v}}{\bar{v}_0} = \omega_0 \exp[-\mathcal{C}(1 + \alpha)/2], \quad (34)$$

where  $\omega_0 \equiv \omega(t = 0)$ , so that

$$\mathcal{C} = \frac{2}{1 + \alpha} \ln \left( 1 + \frac{1 + \alpha}{2} \omega_0 t \right). \quad (35)$$

The corresponding time evolution is

$$\frac{n}{n_0} = \left[ 1 + \frac{1 + \alpha}{2} \omega_0 t \right]^{-\frac{2}{1 + \alpha}} \quad (36)$$

$$\frac{\bar{v}}{\bar{v}_0} = \left[ 1 + \frac{1 + \alpha}{2} \omega_0 t \right]^{\frac{1 - \alpha}{1 + \alpha}}. \quad (37)$$

Without knowing the detailed form of the one-particle distribution function  $f_1$ , it is thus possible to conclude about the time decay of  $n$  and  $\bar{v}$ , which appear to obey algebraic laws in the long time limit [ $n(t) \propto t^{-\xi}$  and  $\bar{v}(t) \propto t^{-\gamma}$ , with  $\xi = 2/(1 + \alpha)$  and  $\gamma = (\alpha - 1)/(\alpha + 1)$ ]. The exponents  $\xi$  and  $\gamma$  are consequently simply related to the unknown quantity  $\alpha$ , for which a perturbative expansion will be put forward in section III before a numerical investigation in

section IV. Moreover, if the initial velocity distribution is of finite support (i.e. vanishes outside a sphere of given velocity  $v^*$ ),  $\bar{v}$  fulfills the bound  $\bar{v} \leq v^*$  so that  $\gamma$  is necessarily positive (or  $\alpha \geq 1$ ). In the framework of Boltzmann's equation, it will be shown in appendix A that the quantity  $\alpha$  is necessarily larger than 1. For the specific initial condition where all particles have the same kinetic energy at  $t = 0$ ,  $\bar{v}^2 = \langle v^2 \rangle$  is time-independent, and (37) implies that  $\alpha = 1$ . From Eq. (36), we therefore obtain the time evolution for this situation

$$\frac{n}{n_0} = \frac{1}{1 + \omega_0 t}, \quad (38)$$

which is exact within the scaling theory. This relation *a priori* holds in any dimension, except for  $d = 1$  where the corresponding initial velocity distribution is the symmetric discrete bimodal function  $\pm c$ , for which the scaling ansatz underlying our approach fails (see the discussion at the end of the present section).

Inserting the scaling forms (27) and (28) into the first equation of the hierarchy (18) imposes the following constraint on the decay exponents:  $\xi + \gamma = 1$ . This scaling relation may be simply obtained by elementary dimensional analysis [4, 5, 6, 9, 10], and may be considered as the compatibility condition of the hierarchy with the self-similar scaling solutions [12]. It is moreover identically fulfilled by the expressions (36) and (37). Under the constraint  $\xi + \gamma = 1$ , the remaining equations of the hierarchy ( $k > 1$ ) turn out to be compatible with (28) with the additional information that the collision term on the lhs of (18) decays like  $t^{-\gamma-d\xi}$  whereas the remaining terms are associated with a power  $1/t$ . Given that  $\gamma + d\xi = 1 + (d-1)\xi \geq 1$ , this collision term is asymptotically irrelevant except in one dimension where it remains of the same order as the dominant ones ( $1/t$ ). We therefore recover the conclusions obtained by considering the formal Grad limit, with distribution functions expected to obey a Boltzmann-like equation. This analysis points to the relevance of Boltzmann equation for  $d > 1$ , a point which is further corroborated by the numerical results given in section IV.

It is interesting to note that both Eq. (38) and the relation  $\xi + \gamma = 1$  do not hold in 1D for discrete initial velocity distributions. In the symmetric situation of a bimodal distribution, the average kinetic energy per particle is conserved (so that  $\gamma = 0$ ), whereas the density decays as  $1/\sqrt{t}$  (i.e.  $\xi = 1/2$  [1]). The scaling assumption (28) is consequently incorrect in the specific situation of discrete distributions in 1D, but valid for continuous distributions [6]. To be more specific, the scaling form (28) implies that the collision frequency scales with time like  $\omega \propto n\bar{v}$ . On the other hand, from the analytical solution of the bimodal  $\pm c$  situation [1], we obtain  $\omega \propto n^2\bar{v}$  with  $\bar{v} = c$ . This discrepancy is the signature of dynamical correlations in the latter discrete case. These correlations are responsible for the breakdown of (28), and in addition violate molecular chaos. For continuous velocity distributions, again in 1D, molecular chaos also breaks down while the scaling (28) is correct. As a consequence, the exponents obtained at the Boltzmann level differ from the exact ones (see the discussion in the last paragraph of section III), whereas the relation  $\xi + \gamma = 1$  holds.

### III. BOLTZMANN KINETIC EQUATION

This section is devoted to the analysis of the decay dynamics within the molecular chaos framework [13] of the homogeneous non-linear Boltzmann equation. No exact solution could be obtained, and our goal is to derive accurate approximate predictions for the scaling exponents  $\xi$  and  $\gamma$  of the density and root mean squared velocity.

Before considering the kinetic equation obeyed by the rescaled distribution function, it is instructive to rewrite the original homogeneous Boltzmann equation (25) in the form

$$\frac{\partial f_1(\mathbf{v}; t)}{\partial t} = -\nu(\mathbf{v}; t)f_1(\mathbf{v}; t) \quad \text{with} \quad \nu(\mathbf{v}_1; t) = \left[ \sigma^{d-1} \int d\hat{\sigma} (\hat{\sigma} \cdot \hat{\mathbf{v}}_{12}) \theta(\hat{\sigma} \cdot \hat{\mathbf{v}}_{12}) \right] \int d\mathbf{v}_2 |\mathbf{v}_{12}| f_1(\mathbf{v}_2; t) \quad (39)$$

where in the last equation, the term in brackets may be computed explicitly as function of dimension (it is understood that the unit vector  $\hat{\mathbf{v}}_{12}$  denotes an arbitrary direction). For our purpose, it is sufficient to notice that at all times, the collision frequency  $\nu(\mathbf{v}; t)$  of the population having velocity  $\mathbf{v}$  remains finite in the limit  $v \rightarrow 0$ , provided the first moment of  $f_1$  exists. In this situation, Eq. (39) implies that  $f_1(\mathbf{v}; t)/f_1(\mathbf{v}; 0)$  admits a finite limit for  $v \rightarrow 0$ , or equivalently, it may be stated that if the initial velocity distribution behaves like  $v^\mu$  near the velocity origin, this feature is preserved by the Boltzmann dynamics. Previous works have shown accordingly that the scaling exponents  $\xi$  and  $\gamma$  depend on the exponent  $\mu$  [4, 6, 9, 10].

Making use of relations (29) and (30), insertion of the scaling form (27) into the Boltzmann equation leads to

$$\left[ 1 + \left( \frac{1-\alpha}{2} \right) \left( d + c_1 \frac{d}{dc_1} \right) \right] \tilde{f}_1(c_1) = \tilde{f}_1(c_1) \int d\mathbf{c}_2 \frac{c_{12}}{\langle c_{12} \rangle} \tilde{f}_1(c_2), \quad (40)$$

where we have assumed an isotropic velocity distribution  $[\tilde{f}_1(\mathbf{c}) = \tilde{f}_1(c)]$  and introduced the average  $\langle(\dots)\rangle = \int(\dots)\tilde{f}_1(c_1)\tilde{f}_1(c_2)d\mathbf{c}_1d\mathbf{c}_2$ .  $\langle c_{12} \rangle$  is therefore the rescaled collision frequency. Once  $\mu$  has been chosen, Eq. (40) admits a solution for a unique value of  $\alpha$ . We show in appendix A that the inequality  $\alpha > 1$  necessarily holds.

Irrespective of  $\alpha$ , the large velocity behaviour of  $\tilde{f}_1$  may be obtained following similar lines as in [4, 5, 9, 14, 15]: it is possible to integrate formally (40) and cast  $\tilde{f}_1$  into

$$\frac{\tilde{f}_1(c)}{\tilde{f}_1(c')} = \left(\frac{c}{c'}\right)^{-\frac{2+d(1-\alpha)}{1-\alpha}} \exp \left[ \frac{2}{1-\alpha} \frac{1}{\langle c_{12} \rangle} \int_{c'}^c \frac{\tilde{\nu}(c'')}{c''} dc'' \right]. \quad (41)$$

In this equation,  $\tilde{\nu}$  is itself a functional of  $\tilde{f}_1$ :

$$\tilde{\nu}(c_1) = \int c_{12} \tilde{f}_1(c_2) d\mathbf{c}_2, \quad (42)$$

such that  $\tilde{\nu}(c)/c$  goes to a finite limit for  $c \rightarrow \infty$ . We therefore obtain the large velocity tail

$$\tilde{f}_1(c) \propto c^{-\frac{2+d(1-\alpha)}{1-\alpha}} \exp \left( -\frac{2}{\alpha-1} \frac{c}{\langle c_{12} \rangle} \right) \quad \text{for} \quad c \rightarrow \infty. \quad (43)$$

In one dimension, we recover the results of references [4] and [9]. In [4, 5], an approximation was derived for  $\alpha$  [or equivalently  $\xi = 2/(1+\alpha)$ ] by assuming that the large velocity behaviour of  $\tilde{f}_1$  could hold for the whole velocity spectrum. In this picture, the power of  $c$  appearing on the rhs of Eq. (43) is equated to the exponent  $\mu$  characteristic of the small velocity behaviour (imposed by the initial distribution chosen, see above), with the result

$$\alpha = 1 + \frac{2}{\mu + d} \quad \text{or} \quad \xi = \frac{2d + 2\mu}{2d + 2\mu + 1}. \quad (44)$$

This prediction encodes the correct dependence on  $\mu$  and dimension ( $\xi$  increases when  $\mu$  or  $d$  increase), and turns out to have an accuracy of order 10% when compared to the numerical results [10]. In the limit of large dimension, we obtain from (44)  $\xi \sim 1 - (2d)^{-1}$ , whereas Krapivsky and Sire have shown that  $\xi \sim 1 - d^{-1}(1 - 1/\sqrt{2})$ , also in the framework of the Boltzmann equation. The remainder of this section is devoted to the derivation of a more precise value for  $\alpha$ , which furthermore coincides with the exact  $1/d$  correction for  $d \rightarrow \infty$ .

Invoking the identity

$$\int d\mathbf{c} c^p \left( d + c \frac{d}{dc} \right) \tilde{f}_1(\mathbf{c}) = -p \langle c^p \rangle, \quad (45)$$

the energy dissipation parameter  $\alpha$  may be given the set of equivalent expressions:

$$\alpha = 1 + \frac{2}{p} \left( \frac{\langle c_{12} c_1^p \rangle}{\langle c_{12} \rangle \langle c_1^p \rangle} - 1 \right), \quad \forall p \geq 0. \quad (46)$$

A particularly useful relation between  $\alpha$  and moments of  $\tilde{f}_1$  follows from considering the limit  $c_1 \rightarrow 0$  of (40): we get

$$\alpha = 1 + \frac{2}{\mu + d} \left( 1 - \frac{\langle c_1 \rangle}{\langle c_{12} \rangle} \right). \quad (47)$$

The (infinite) family of relations (47) and (46) is equivalent to the original integro-differential equation (40), and well suited to a perturbative analysis. To this end, a systematic approximation of the isotropic function  $\tilde{f}_1$  can be found by expanding it in a set of Sonine polynomials [16]:

$$\tilde{f}_1(c) = \mathcal{M}(c) \left[ 1 + \sum_{n=1}^{\infty} a_n S_n(c^2) \right]. \quad (48)$$

These polynomials are orthogonal with respect to the Gaussian weight

$$\mathcal{M}(c) = \left( \frac{d}{2\pi} \right)^{d/2} e^{-dc^2/2}, \quad (49)$$



and the first few read

$$S_0(x) = 1 \quad (50)$$

$$S_1(x) = \frac{d}{2}(-x + 1) \quad (51)$$

$$S_2(x) = \frac{d^2}{8}x^2 - \frac{d(d+2)}{4}x + \frac{d(d+2)}{8}. \quad (52)$$

The coefficients  $a_n$  follow from the orthogonality relation  $\int S_n(c^2)S_m(c^2)\mathcal{M}(c)d\mathbf{c} \propto \delta_{nm}$ : In particular,

$$a_1 = \frac{2}{d}\langle S_1(c^2) \rangle = \frac{2}{d}(1 - \langle c^2 \rangle) = 0 \quad (53)$$

from the definition of rescaled velocities (26). The first non-Gaussian correction is thus embodied in  $a_2$ , that is proportional to the fourth cumulant (kurtosis) of the velocity distribution:

$$a_2 = \frac{d^2}{3} [\langle c_i^4 \rangle - 3\langle c_i^2 \rangle^2] = \frac{d}{d+2} \langle c^4 \rangle - 1, \quad (54)$$

with  $c_i$  a Cartesian component of  $\mathbf{c}$ . Upon truncating Eq. (48) at a finite order  $n$ , we obtain a regular velocity distribution near  $c = 0$ . We consequently restrict our analysis to the case  $\mu = 0$  (the dependence on  $\mu$  has been considered in [10]).

It is also noteworthy that any truncation of (48) at arbitrary order  $n$  leads to a Gaussian high energy behaviour, incompatible with the result (43) corresponding to an overpopulated tail with respect to the Maxwellian. However, it will be shown in section IV that the difference between the truncated expansion (48) and the numerical velocity distribution becomes manifest far in the tail, where the distribution has reached very low probabilities. Consequently, when the moment involved in (46) and (47) are evaluated from the truncation of (48), the accuracy of the result is expected to be better for low orders  $p$  in (46). Hence the privileged role played by (47), which is of lower order than any of the identities (46). In practice, upon truncating (48) at order  $n$ , the  $n$  unknowns  $\alpha, a_2, \dots, a_n$  are computed evaluating the corresponding moments appearing in (47) and in  $n-1$  of the relations (46), among which it is convenient to retain the  $n-1$  even values of  $p$  ( $p=0$  excluded). Truncation of (48) at order  $n=2$  yields precise predictions for  $\alpha$  and  $\tilde{f}_1$ , and already at Gaussian order,  $\alpha$  turns out to be very close to its numerical counterpart: Setting  $n=0$  (or equivalently  $n=1$  since  $a_1 \equiv 0$ ) in (48), we obtain immediately the zeroth order approximation

$$\alpha = \alpha_0 = 1 + \frac{2}{d} \left( 1 - \frac{\sqrt{2}}{2} \right) \quad (55)$$

which corresponds to

$$\xi = \xi_0 = \frac{2}{1 + \alpha_0} = \frac{2d}{2(d+1) - \sqrt{2}}. \quad (56)$$

For large dimensions, this estimation goes to unity, with the exact  $1/d$  correction computed in [9]

$$\xi = 1 - \frac{1}{d} \left( 1 - \frac{\sqrt{2}}{2} \right) + \mathcal{O}\left(\frac{1}{d^2}\right). \quad (57)$$

This behaviour turns out to be “universal”, in the sense that the  $\mu$  dependence does not appear at this order [10].

We shall also be interested in the non-Gaussian features of the velocity distribution, that we quantify by the fourth cumulant  $a_2$ . The (cumbersome) calculations at second order in Sonine expansion are detailed Appendix B. We obtain

$$a_2 = 8 \frac{d(2\sqrt{2} - 3)}{4d^2 + d(6 - \sqrt{2})} \quad (58)$$

$$\alpha_2 = \alpha_0 + \frac{\sqrt{2}}{16d} a_2. \quad (59)$$

The corresponding density exponent follows from  $\xi_2 = 1/(1 + \alpha_2)$  as before. For  $d \rightarrow \infty$ ,  $a_2 \sim 2(3 - 2\sqrt{2})d^{-1}$ , irrespective of  $\mu$  [10] which reinforces the “universal” nature of large  $d$ . The correction to  $\xi$  carried by  $a_2$  behaves

as  $1/d^2$  in this limit, and does not affect the  $1/d$  terms which still coincide with the exact behaviour (57). Both predictions (55) and (59) are such that  $\alpha > 1$ , which is required to obtain a normalizable distribution in (41) and (43).

The second order expansion considered here may be improved by consideration of higher order Sonine terms and inclusion of non-linear terms in  $a_2$ . In the related context of inelastic hard spheres, the limitation of working at linear order in  $a_2$  with neglect of Sonine terms of order  $n \geq 3$  may be found in [17]. Alternatively, keeping non linear terms in  $a_2$  and neglecting again Sonine terms of order  $n \geq 3$  leads to multiple solutions. A stability analysis is then required to determine which one is stable, as discussed in [18].

Here, the value obtained for  $a_2$  is quite small (see below). Our approximate expressions are accurate when compared to the full numerical solution of Boltzmann's equation, so that we did not calculate any higher order coefficients, nor consider non linear terms in  $a_2$ . The existing body of literature reports, within Boltzmann framework, numerical exponents in 1D that are in excellent agreement with our predictions, already at zeroth order. For the case  $\mu = 0$ , expressions (56) and (59) give  $\xi_0 \simeq 0.773$  and  $\xi_2 \simeq 0.769$  whereas the numerical result obtained in [9] is  $\xi \simeq 0.769$ . These exponents are close to their counterparts extracted numerically from the exact dynamics ( $0.785 \pm 0.005$  in [6], and more recently  $0.804$  [19]). The difference between the exact exponents and those obtained assuming molecular chaos is consistent with the conclusion of section II: In 1 dimension, the factorization of the two-body distribution  $\tilde{f}_2$  underlying Boltzmann ansatz is not an exact property of the distributions obeying hierarchy (18). On the other hand, for  $d \geq 1$ , the molecular chaos exponents are expected to become exact. This property is illustrated in the next section.

#### IV. SIMULATION RESULTS

The numerical results presented in this section correspond to the situation  $\mu = 0$ , unless stated. We refer to [10] for the case of diverging ( $\mu < 0$ ) or depleted ( $\mu > 0$ ) velocity distributions near  $v = 0$ .

##### A. The numerical methods

We follow two complementary numerical routes. First, we solve the time-dependent homogeneous Boltzmann equation by means of the Direct Simulation Monte Carlo method (DSMC), originally developed to study ordinary gases [20]. This scheme, where a suitable Markov chain is constructed, has been extended to deal with inelastic collisions [21, 22] and is easily modified to describe the situation under study here, which does not conserve the total number of particles. Restricting to a spatially homogeneous system, the algorithm is especially easy to implement, and may be summarized as follows: among  $N_0$  initial particles having a given velocity distribution, a pair  $(i, j)$  is chosen at random, and removed from the system with a probability proportional to  $|\mathbf{v}_{ij}|$ . The (suitably renormalized) time variable is then incremented by the amount  $(N^2 |\mathbf{v}_{ij}|)^{-1}$ , where  $N$  is the number of particles remaining in the system, before another pair is drawn etc... This scheme provides the numerical exact solution of Eq. (39), and allows to test the validity of the approximations put forward in section III [essentially: Truncation at second order in expansion (48) supplemented with calculations performed at linear order in the fourth cumulant  $a_2$ , see Appendix B]. A precise analysis of the late time dynamics (and especially the computation of velocity distributions) suffers from the concomitant low number of particles left, and the statistical accuracy is improved by averaging over independent realizations.

The second numerical method (Molecular Dynamics [23]) consists of integrating the exact equations of motion for an assembly of spheres confined in a (hyper)-cubic box with periodic boundary conditions. This route assesses the validity of the approach relying on the homogeneous Boltzmann equation, but does not offer the same accuracy as DSMC, nor the possibility to follow the evolution over comparable times. In particular, once the mean-free-path  $\lambda$ , which grows rapidly as  $t^\xi$ , becomes of the order of the box size  $L$ , the subsequent evolution suffers from finite size effects and should be discarded: When  $\lambda > L$ , the algorithm used is unable to find collision events for those particles which make more than one free flight round on the torus topologically equivalent to the simulation box, which causes a spurious slowing down of the dynamics. It is then tempting to reduce  $\lambda$  by increasing particles diameter  $\sigma$ , but then finite (and necessarily transient) density effects –incompatible with the scaling assumption (28)– may also arise if the packing fraction  $\phi$ , proportional to  $n\sigma^d$ , is not low enough. Simulating explicitly the limit of point particles, the DSMC scheme considered here is free of this defect. The initial number of particles considered in MD needs to be large to allow the system to enter the scaling regime before finite-size effects become dominant: we considered systems with  $N = 5 \cdot 10^4$  to  $N = 5 \cdot 10^5$  spheres initially (compared to  $N = 10^6$  to  $10^8$  in DSMC).

## B. Dynamic scaling behaviour

The results of two-dimensional DSMC and MD simulations are shown in Figure 1, where the quantity on the  $x$  axis is expected to scale like real time  $t$  from the scaling relation  $\xi + \gamma = 1$ . This log-log plot is a direct probe of the exponent  $\xi$ , from the slope measured. Both MD and DSMC methods give compatible results, with the possibility to follow the dynamics over a longer time interval in DSMC. The departure observed for  $n_0/n \simeq 200$  corresponds to the slowing down of MD dynamics resulting from finite-size effects (see Figure 2 below). The theoretical predictions at zeroth and second order are very close ( $\xi_0 = 0.872$  and  $\xi_2 = 0.870$ ), and in excellent agreement with the simulation results over several decades. On a similar graph as Fig. 1, the kinetic “temperature”  $\bar{v}^2$  exhibits a lower law behaviour (not shown) with an exponent  $-2\gamma$  in good agreement with the theoretical prediction ( $\gamma \simeq 0.13$  in 2D). Moreover, the exponents obtained analytically and numerically are compatible to those reported in the literature ( $\xi \simeq 0.89$  in [4] and  $\xi \simeq 0.87(5)$  using a multi-particle lattice gas method [24]).

The time evolution of inverse density and inverse typical velocity square is shown in Figure 2, where considering  $n_0/n - 1$  and  $\bar{v}_0^2/\bar{v}^2 - 1$  instead of  $n_0/n$  and  $\bar{v}_0^2/\bar{v}^2$  allows to probe the short time behaviour. Unless stated, the initial velocity distribution is an isotropic Gaussian. From Eqs. (29) and (30),  $n$  and  $\bar{v}^2$  evolve linearly with  $t$  for  $\omega_0 t \ll 1$  [see also (36) and (37)]; the same holds for inverse density and inverse typical velocity squared, which is indeed observed in Fig. 2. MD and DSMC result super-impose, except at late times where MD dynamics suffers from the slowing down discussed previously. For both numerical methods, the scaling relation  $\xi + \gamma = 1$  is well obeyed, in principle at late times only, in the scaling regime. Special combinations of  $n$  and  $\bar{v}$  can however be constructed with the requirement to match the short time evolution with the scaling behaviour. One of these quantities is displayed in Fig. 3, with a resulting scaling regime extending over more than 10 decades in time. In Fig. 4, we not only test the validity of the theoretical scaling exponents, but also the full time dependence as predicted by Eqs. (36) and (37). In order to improve the agreement between theory and simulation (which holds over more than 6 orders of magnitude in time), the system has been left time to enter the scaling regime: The time origin  $t = 0$  has been chosen when 80% of the particles originally present have disappeared. The corresponding reference configuration (with subscripts 0) thus differs from the ones considered previously.

## C. Velocity distribution in the scaling regime

In order to understand the reasons for the good agreement between our theoretical predictions and the simulations, we now consider the velocity distribution, restricting to Monte Carlo results (leading to similar conclusions, MD is much more demanding on CPU time and does not allow to investigate detailed features of  $\tilde{f}_1$  with the same accuracy). After a transient where the probability distribution function  $\tilde{f}_1$  evolves with time, a well defined scaling regime is reached with a time independent  $\tilde{f}_1(\mathbf{c})$  shown in Fig. 5 together with the Sonine prediction pushed at second order. The agreement is remarkable, and it is also observed that the Gaussian approximation is already close to the asymptotic rescaled velocity distribution, which is quite surprising in a kinetic process extremely far from equilibrium, with furthermore no conservation laws. Given that our perturbative analytical work relies on the calculation on low order moments of  $\tilde{f}_1$ , this explains the accuracy of the zeroth order predictions  $\alpha_0$  and  $\xi_0$ . From Eq. (43), we expect the differences between the Sonine expansion and the numerical distribution to become visible in the high energy tail, which is confirmed by Fig. 6. As predicted,  $\tilde{f}_1$  is overpopulated with respect to the Gaussian, and displays a high velocity tail of the form (43) (see the inset).

## D. Evolution toward the asymptotic solutions

Before the scaling regime is attained,  $\tilde{f}_1$  is time-dependent, as shown in Fig. 7, where the distributions at different times have been renormalized by  $\mathcal{M}$  to emphasize the building-up of non-Gaussianities. The evolution towards the scaling solution  $1 + a_2 S_2$  can be observed. With respect to the Gaussian,  $\tilde{f}_1$  is at all times overpopulated both at large and small velocities (which may be related to the positive sign of  $a_2$  for the latter case); normalization is ensured by an under-population at intermediate velocities. Figures 5, 6 and 7 show that the indirect measure of  $a_2$  through the non-Gaussian character of  $\tilde{f}_1/\mathcal{M}$  agrees with the theoretical prediction, but it is also possible to compute directly  $a_2$  in the simulations through its definition as a fourth cumulant [Eq. (54)]. It turns that both methods are numerically fully compatible. Moreover, the Sonine expansion (48) truncated at  $n = 2$  holds at any time, even in the transient regime, with the time dependent fourth cumulant  $a_2$  measured from (54) (see Fig. 8). This result is not a priori expected and points to the relevance of the expansion (48). We did not try to solve analytically the homogeneous time-dependent Boltzmann equation within the same framework as in the scaling regime, so that we do not have any

prediction for the (transient) time-dependence of  $a_2$  and  $\alpha$ . However, as shown in the inset of Fig. 8, the relation (B10) (which reads in 2D  $\alpha = 5/4 + 7a_2/16$ ) remarkably holds for all time. Here, the energy dissipation parameter  $\alpha$  has been computed through the ratio  $\langle c_{12} c_1^2 \rangle / (\langle c_{12} \rangle \langle c_1^2 \rangle) = \langle c_1^2 \rangle_{\text{coll}} / \langle c_1^2 \rangle$ , where  $\langle c_1^2 \rangle_{\text{coll}}$ , the mean energy dissipated in a collision is computed in the simulations and normalized by the time-dependent mean kinetic energy per particle  $\langle c_1^2 \rangle$ .

### E. A final remark: Identification of “isobestic” points

For  $\mu = 0$ , Figure 7 indicates that during the transient evolution toward scaling, the distributions of reduced velocities have fixed points (for a given initial velocity distribution, the curves corresponding to  $\tilde{f}_1$  at different times all pass through common points, that we called isobestic points). This feature has been observed for all initial distributions investigated and appears to be a systematic property of the dynamics, which still holds for non vanishing values of  $\mu$  (see Fig. 9). We have no analytical explanation for this observation.

## V. CONCLUSION

An analytical derivation of the equations governing the dynamics of an infinite system of spherical particles in a  $d$ -dimensional space, moving freely between collisions and annihilating in pairs when meeting, has been obtained. The hierarchy equations obeyed by the reduced distributions  $f_k(1, 2, \dots, k; t)$  have been derived. In the Grad limit, this hierarchy formally reduces to a Boltzmann-like hierarchy for dimensions  $d > 1$ . If these reduced distributions  $f_k^B$  factorize at the initial time, this factorization remains valid for all times and the whole hierarchy reduces to one non-linear equation.

In the long time limit, the ratio of the particle radius to the mean-free path vanishes. A scaling analysis of the exact homogeneous hierarchy equations has been performed. Self-similar reduced distributions in which the time dependence has been absorbed into the density  $n(t)$  and the root mean-square velocity  $\bar{v}(t)$  were introduced. As a result, the exponents  $\xi$  and  $\gamma$  describing the decay with time of  $n(t)$  and  $\bar{v}(t)$  depend only upon one single parameter  $\alpha$ , related to the dissipation of energy. Moreover, it turns out that in dimension higher than 1, the terms responsible for the violation of molecular chaos are asymptotically irrelevant. Therefore, we recover the conclusions reached in the formal Grad limit and thus, the Boltzmann equation becomes exact in the long time limit in dimensions higher than 1. The above arguments give a first principle justification for the use of the Boltzmann equation approach for  $d > 1$ , as well as its limitations, in ballistic annihilation problems, an issue that has been overlooked so far. However, as discussed above, this scaling analysis is incorrect for a 1 dimensional system with discrete initial velocity distribution, a situation for which the scaling assumption underlying our approach fails.

The Boltzmann equation has been solved within an expansion in Sonine polynomials  $S_n$ . Truncation to order  $n = 2$ , provides the first non-Gaussian corrections to the scaled velocity distribution, and leads to analytical predictions for the exponents  $\xi$  and  $\gamma$  as a function of  $d$ . For large dimension  $d$ , these predictions coincide with the exact  $1/d$  correction to the naive mean field values ( $\xi = 1$  and  $\gamma = 0$ ), calculated in [9]. The above analytical predictions are in remarkable agreement with the results of extensive numerical simulations we have performed for two dimensional systems (implementing the complementary Monte Carlo and Molecular Dynamics techniques). In 1D for regular continuous velocity distributions, it is noteworthy that they are in excellent agreement with the numerical solution of the Boltzmann equation, and quite close to the exact values obtained with Molecular Dynamics (4% difference). This last point was unexpected since molecular chaos breaks in 1D. Finally, the time dependence of the reduced velocity distribution function shows an unexplained and remarkable feature, with the existence of fixed (“isobestic”) points, irrespective of initial conditions.

Acknowledgments: We would like to thank F. Coppex for a careful reading of the manuscript, T. van Noije, A. Barrat, F. van Wijland and A. Santos for useful discussions. E.T. acknowledges the hospitality of the Theoretical Physics Department (Genève) where part of this work was performed. J.P. and E.T. benefited from the financial support of the “Programme d’Action Intégrée Franco-Polonais Polonium” (contract 03990WF). M.D. acknowledges the support of the Swiss National Science Foundation and of the CNRS through the attribution of a “poste de chercheur associé”.

## APPENDIX A

Within Boltzmann's kinetic equation, we show in this appendix that  $\alpha > 1$ . To this end, Eq. (40) is rewritten in the form

$$\tilde{f}_1(c_1) + \left(\frac{1-\alpha}{2}\right) \text{div}_{\mathbf{c}_1} \left(\mathbf{c}_1 \tilde{f}_1(c_1)\right) = \tilde{f}_1(c_1) \int d\mathbf{c}_2 \frac{c_{12}}{\langle c_{12} \rangle} \tilde{f}_1(c_2), \quad (\text{A1})$$

and integrated with weight  $\psi(c_1) d\mathbf{c}_1$ , where we choose  $\psi(c) = c^{2/(1-\alpha)}$ . Assuming that the moment  $\int \psi \tilde{f}_1$  exists, we obtain after an integration by parts (neglecting surface terms)

$$0 = \int d\mathbf{c}_1 d\mathbf{c}_2 \psi(c_1) \frac{c_{12}}{\langle c_{12} \rangle} \tilde{f}_1(c_1) \tilde{f}_1(c_2). \quad (\text{A2})$$

The right hand side of Eq. (A2) is a strictly positive quantity [except when  $\tilde{f}_1(c) = \delta(c)$ ], which leads to a contradiction. We therefore conclude that the quantity  $\int \psi \tilde{f}_1$  does not exist. Remembering that  $\psi(c) \tilde{f}_1(c) \sim c^{\mu+2/(1-\alpha)}$  near the velocity origin, the divergence of  $\int \psi \tilde{f}_1$  implies

$$\frac{2}{1-\alpha} + d - 1 + \mu < -1. \quad (\text{A3})$$

Supplementing this condition with the normalization constraint  $\mu > -d$ , we obtain  $\alpha > 1$ . The physical meaning of this condition is that the typical kinetic energy dissipated per particle in a collision is larger than the average kinetic energy of the system at the same time. The temperature  $\bar{v}^2$  is therefore a decreasing function of time.

## APPENDIX B: SECOND ORDER TRUNCATED SONINE EXPANSION

In this Appendix, we calculate the dominant deviation of  $\tilde{f}_1$  from the Gaussian shape, and the associated energy dissipation parameter  $\alpha$  by setting  $\tilde{f}_1(c) = \mathcal{M}(c) \{1 + a_2 S_2(c^2)\}$ . The moments appearing in (47) and (46) with  $p = 2$  are then computed as a function of  $a_2$ . Upon writing

$$\alpha = 1 + \frac{2}{\mu + d} \left(1 - \frac{\langle c_1 \rangle}{\langle c_{12} \rangle}\right) = \frac{\langle c_{12} c_1^2 \rangle}{\langle c_{12} \rangle \langle c_1^2 \rangle}, \quad (\text{B1})$$

the last equality provides an equation for  $a_2$  which is solved so that  $\alpha$  is finally explicitly known as a function of input parameters  $\mu$  and dimension  $d$ . As in the main text, the angular brackets denote averages with weight  $\tilde{f}_1(c_1) \tilde{f}_1(c_2)$

$$\langle \dots \rangle = \int (\dots) \tilde{f}_1(c_1) \tilde{f}_1(c_2) d\mathbf{c}_1 d\mathbf{c}_2 \quad (\text{B2})$$

$$= \int (\dots) \mathcal{M}(c_1) \mathcal{M}(c_2) \{1 + a_2 [S_2(c_1^2) + S_2(c_2^2)]\} d\mathbf{c}_1 d\mathbf{c}_2 + \mathcal{O}(a_2^2). \quad (\text{B3})$$

In the following, non-linear terms of order  $a_2^2$  will be neglected. In the spirit of [25], it is convenient to introduce center-of-mass and relative velocities  $\mathbf{c}_1 = \mathbf{C} + \mathbf{c}_{12}/2$ ;  $\mathbf{c}_2 = \mathbf{C} - \mathbf{c}_{12}/2$  and to define the generic moments

$$M_{np} = \langle c_{12}^n C^p \rangle \quad (\text{B4})$$

$$= \int d\mathbf{c}_{12} d\mathbf{C} c_{12}^n C^p \left(\frac{d}{2\pi}\right)^d e^{-d\mathbf{c}_{12}^2/4 - d\mathbf{C}^2} \left\{1 + a_2 \left[\frac{d^2}{8} (c_1^4 + c_2^4) - \frac{d(d+2)}{4} (c_1^2 + c_2^2) + \frac{d(d+2)}{4}\right]\right\} \quad (\text{B5})$$

From  $c_1^4 + c_2^4 = 2C^4 + 2(\mathbf{C} \cdot \mathbf{c}_{12})^2 + c_{12}^4/8 + C^2 c_{12}^2$ , the term  $(\mathbf{C} \cdot \mathbf{c}_{12})^2$  appearing under the integral sign in (B5) becomes  $C^2 c_{12}^2/d$  for symmetry reasons, and making use of  $c_1^2 + c_2^2 = 2C^2 + c_{12}^2/2$ , the variables  $\mathbf{c}_{12}$  and  $\mathbf{C}$  decouple in (B5). The resulting integrals yield

$$\frac{M_{np}}{M_{np}^0} = \frac{\langle c_{12}^n C^p \rangle}{\langle c_{12}^n C^p \rangle_0} = 1 + \frac{a_2}{16d} \{d(n^2 + p^2) - 2d(n + p) + 2np(d + 2)\} + \mathcal{O}(a_2^2). \quad (\text{B6})$$

In this equation, the subscript 0 refers to averages with Gaussian measure (formally  $a_2 = 0$ ):

$$\langle c_{12}^n C^p \rangle_0 = (\sqrt{d})^{-n-p} 2^n \frac{\Gamma\left(\frac{d+n}{2}\right) \Gamma\left(\frac{d+p}{2}\right)}{\Gamma^2(d/2)}, \quad (\text{B7})$$

where  $\Gamma$  is the Euler function. The moments  $\langle c_{12} \rangle$  and  $\langle c_{12} c_1^2 \rangle = \langle c_{12}(c_1^2 + c_2^2) \rangle / 2 = \langle c_{12}^3 \rangle / 4 + \langle c_{12} C^2 \rangle$  appearing in (B1) are then known

$$\frac{\langle c_{12} \rangle}{\langle c_{12} \rangle_0} = 1 - \frac{1}{16} a_2 + \mathcal{O}(a_2^2) \quad (\text{B8})$$

$$\frac{\langle c_{12} c_1^2 \rangle}{\langle c_{12} \rangle_0} = 1 + \frac{1}{2d} + \frac{a_2}{32} \left( 6 + \frac{11}{d} \right) + \mathcal{O}(a_2^2) \quad (\text{B9})$$

$$\Rightarrow \frac{\langle c_{12} c_1^2 \rangle}{\langle c_{12} \rangle \langle c_1^2 \rangle} = 1 + \frac{1}{2d} + \frac{a_2}{8} \left( 2 + \frac{3}{d} \right) + \mathcal{O}(a_2^2). \quad (\text{B10})$$

For an elastic hard sphere fluid at equilibrium (with thus  $a_2 = 0$ ), this last quantity equals  $1 + 1/(2d)$  and represents the ratio of the mean kinetic energy of colliding particles (averaged over successive collision events) to the mean kinetic energy of the population. As expected, this ratio exceeds 1, since typical colliding partners are “hotter” than the mean background. This quantity is easily measured in Molecular Dynamics or Monte Carlo simulations (see e.g. Fig. 8). We also note that the ratio (B8) has been computed in [14] at the same level of approximation in the context of rapid granular flows, with the same result. van Noije and Ernst also reported non Gaussian corrections to the cooling rate  $\gamma$  of an inelastic hard sphere fluid [14]

$$\frac{\gamma}{\gamma_0} = 1 + \frac{3}{16} a_2 + \mathcal{O}(a_2^2) \quad \forall d, \quad (\text{B11})$$

where  $\gamma_0$  denotes the cooling rate evaluated assuming Maxwellian velocity distributions. In terms of the moments  $M_{np}$  introduced in (B4), it can be shown that  $\gamma/\gamma_0 = M_{30}/M_{30}^0$  and it is then easily checked that expression (B6) reduces to (B11) for  $n = 3$  and  $p = 0$ , for arbitrary dimensionality.

The remaining unknown quantity is  $\langle c_1 \rangle$  which may be calculated following similar lines as above:

$$\frac{\langle c_1^n \rangle}{\langle c_1^n \rangle_0} = 1 + \frac{a_2}{8} n(n-2) + \mathcal{O}(a_2^2) \quad (\text{B12})$$

$$\langle c_1^n \rangle_0 = \left( \frac{2}{d} \right)^{n/2} \frac{\Gamma(\frac{d+n}{2})}{\Gamma(\frac{d}{2})}, \quad (\text{B13})$$

from which we extract  $\langle c_1 \rangle = \langle c \rangle$ . As expected, the  $a_2$  correction in (B13) vanishes for  $n = 0$  and  $n = 2$ , which follows respectively from the normalization constraint and the definition (26) of  $\mathbf{c}$  implying  $\langle c^2 \rangle = 1$ . Gathering results, we obtain (58) and (59) from Eqs. (B1).

- 
- [1] Y. Elskens and H.L. Frisch, Phys. Rev. A **31**, 3812 (1985).
  - [2] J. Piasecki, Phys. Rev. E **51**, 5535 (1995).
  - [3] M. Droz, P.A. Rey, L. Frachebourg and J. Piasecki, Phys. Rev. Lett. **75**, 160 (1995).
  - [4] E. Ben-Naim, S. Redner and F. Leyvraz, Phys. Rev. Lett. **70**, 1890 (1993).
  - [5] E. Ben-Naim, P.L. Krapivsky, F. Leyvraz and S. Redner, J. Phys. Chem. **98**, 7284 (1994).
  - [6] P.A. Rey, M. Droz and J. Piasecki, Phys. Rev. E **57**, 138 (1998).
  - [7] Y. Kafri, J. Phys. A: Math. Gen. **33**, 2365 (1999).
  - [8] R.A. Blythe, M.R. Evans and Y. Kafri, Phys. Rev. Lett. **85**, 3750 (2000).
  - [9] P.L. Krapivsky and C. Sire, Phys. Rev. Lett. **86**, 2494 (2001).
  - [10] E. Trizac, Phys. Rev. Lett. **88**, 160601 (2002).
  - [11] D. Ruelle, “Statistical Mechanics” (Mathematical Physics Monograph Series, W.A. Benjamin Inc.), Chapter 7 (1969).
  - [12] E. Trizac and J.-P. Hansen, Phys. Rev. Lett. **74**, 4114 (1995).
  - [13] P. Résibois and M. de Leener, *Classical Kinetic Theory of Fluids*, John Wiley and Sons (1977).
  - [14] T.P.C. van Noije and M.H. Ernst, Gran. Matter **1**, 57 (1998).
  - [15] A. Barrat, T. Biben, Z. Rácz, E. Trizac and F. van Wijland, J. Phys. A **35**, 463 (2002).
  - [16] L. Landau and E. Lifshitz, *Physical Kinetics*, Pergamon Press (1981).
  - [17] J.M. Montanero and A. Santos, Granular Matter **2**, 53 (2000).
  - [18] N.V. Brilliantov and T. Poschel, Phys. Rev. E **61**, 2809 (2000).
  - [19] E. Ben-Naim, MD simulations with 10 runs of  $10^6$  particles, private communication.
  - [20] G. Bird, “Molecular Gas Dynamics” (Oxford University Press, New York, 1976) and “Molecular Gas Dynamics and the Direct Simulation of Gas flows” (Clarendon Press, Oxford, 1994).

- [21] J.M. Montanero, V. Garzó, A. Santos and J.J. Brey, J. Fluid Mech. **389**, 391 (1999).
- [22] A. Frezzotti, Physica A **278**, 161 (2000).
- [23] M.P. Allen and D.J. Tildesley “Computer Simulations of Liquids” (Clarendon Press, Oxford, 1987).
- [24] B. Chopard, A. Masselot and M. Droz, Phys. Rev. Lett. **81**, 1845 (1998).
- [25] I. Pagonabarraga, E. Trizac, T.P.C. van Noije, and M.H. Ernst, Phys. Rev. E **65**, 011303 (2002).

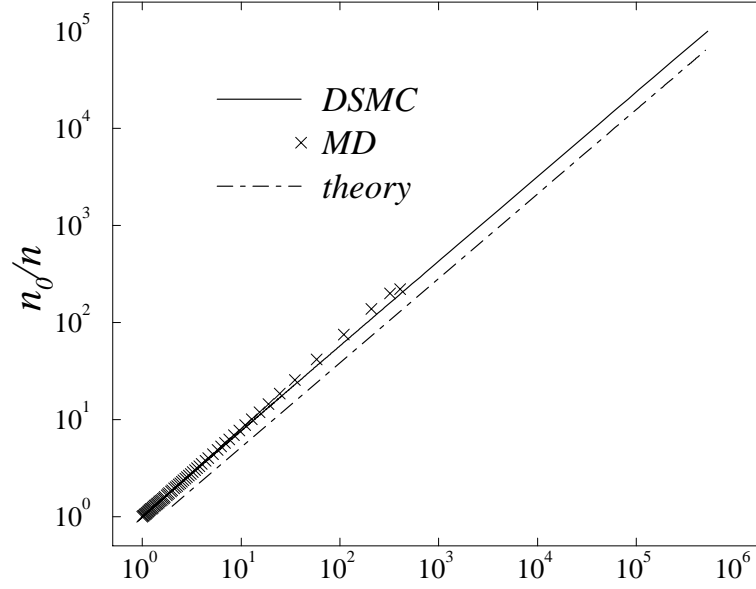


FIG. 1: Inverse density  $n_0/n$  versus  $n_0 \overline{v}_0 / (n \overline{v})$ , for  $d = 2$ . The dotted line has slope  $\xi_2 = 0.87$  [see equation (56)]. Initial number of particles:  $5 \cdot 10^6$  (with a further average over  $10^3$  independent replicas) for DSMC and  $2 \cdot 10^5$  for MD. In both cases, the initial velocity distribution is Gaussian ( $\mu = 0$ ), and the initial configuration used for MD is that of an equilibrium hard disk fluid with packing fraction  $\phi = 0.1$  (chosen low enough to avoid finite packing effects).

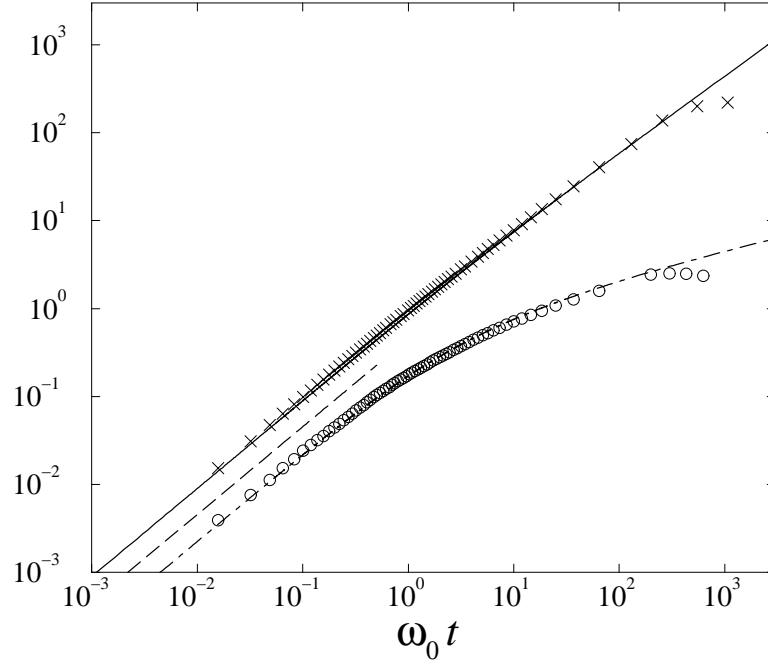


FIG. 2: Plots of  $(n_0/n) - 1$  [upper curve corresponding to DSMC, compared to its MD counterpart (crosses)] and  $(\overline{v}_0/\overline{v})^2 - 1$  (lower dashed curve for DSMC, circles for MD), as a function of time. The dotted line at short times has slope 1.

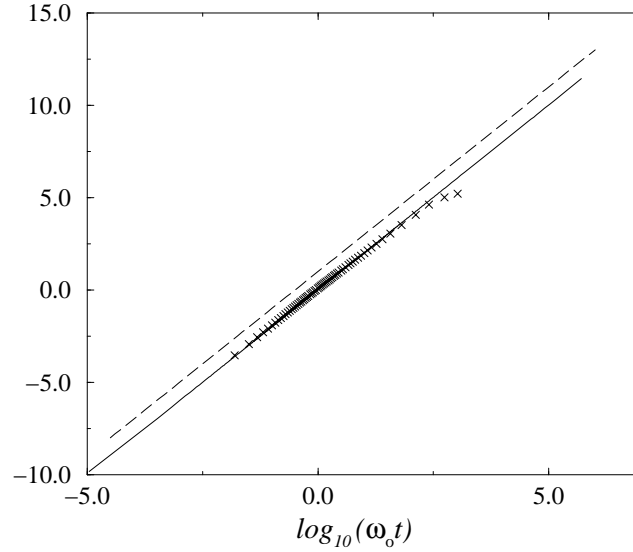


FIG. 3: Plot of  $\log_{10}[n_0/n - 1] + \log_{10}[n_0\overline{v}_0^2/(n\overline{v}^2) - 1]$  on a logarithmic time scale ( $d = 2$ ). DSMC results are represented by the continuous curve, while the crosses correspond to MD. The dashed line has slope 2. At late times, the quantity displayed is expected to behave as  $2\log_{10}(\omega_0 t)$  from the scaling relation  $\xi + \gamma = 1$ . At short times, the same behaviour is observed, for a different reason [see Eqs. (36) and (37)]. The ultimate MD slowing down is again visible.



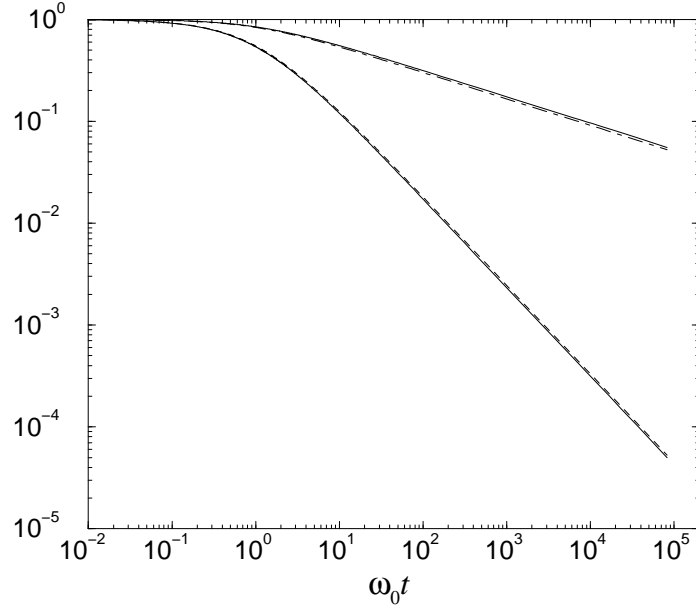


FIG. 4: Time dependence of  $n$  (lower curve) and  $\bar{v}^2$  (upper curve) obtained in Monte Carlo, compared to the dashed curves corresponding to the theoretical predictions (36) and (37), where the energy dissipation coefficient  $\alpha$  is calculated at second order in Sonine expansion [ $\alpha_2 \simeq 1.297$  from Eq. (59)].

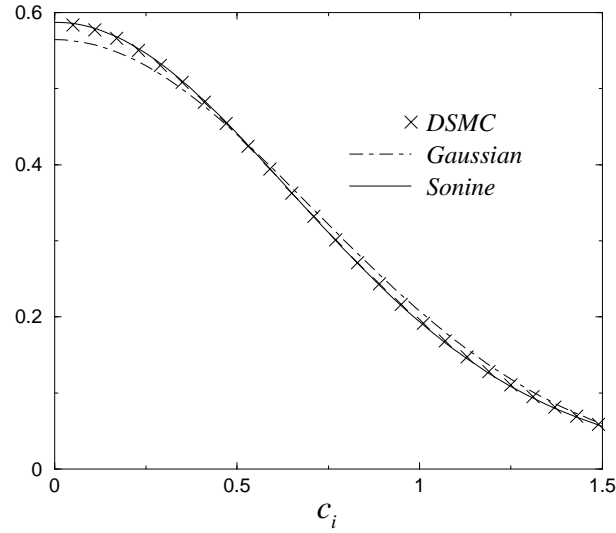


FIG. 5: Probability distribution function  $\tilde{f}_1(c_i)$  of a given Cartesian component  $c_i$  of the rescaled two-dimensional velocity  $\mathbf{c}$ . The time independent distribution obtained in DSMC simulations at late times is compared to the Gaussian  $\mathcal{M}$  and the Sonine expansion truncated at  $n = 2$ , with the fourth cumulant given by Eq. (58) ( $a_2 \simeq 0.109$  for  $d = 2$  and  $\mu = 0$ ). All distributions have variance  $1/2$  so that  $\langle c^2 \rangle = 1$ . The results have been obtained by averaging over 50 replicas of a system with initially  $N = 40 \cdot 10^6$  particles.

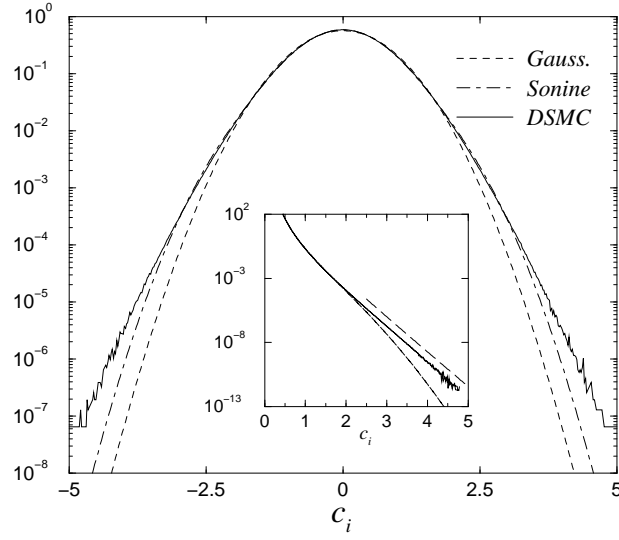


FIG. 6: Same as Figure 5, on a linear-log scale to probe the tails of the distributions. In the inset showing  $c_i^{-4.7} \tilde{f}_1(c_i)$  as a function of  $c_i$ , the dashed curve corresponds to the Gaussian [ $c_i^{-4.7} \mathcal{M}(c_i)$ ] while the straight line is a guide for the eye evidencing a pure exponential behaviour. For  $d = 2$  and  $\mu = 0$ , the exponent  $d + 2/(1 - \alpha)$  appearing in Eq. (43) is close to -4.7 and has been used to rescale the quantity plotted on the  $y$ -axis in the inset.

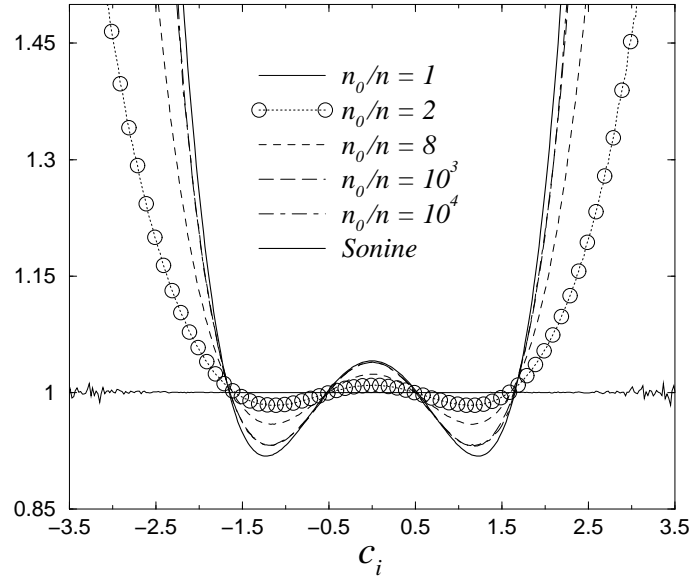


FIG. 7: Plots of  $\tilde{f}(c_i)/\mathcal{M}(c_i)$  versus  $c_i$ , at different times corresponding to the indicated densities. The initial distribution is Gaussian (thus corresponding to the flat curve), and the thick curve is Sonine solution  $1 + a_2 S_2$  with  $a_2$  given by (58).

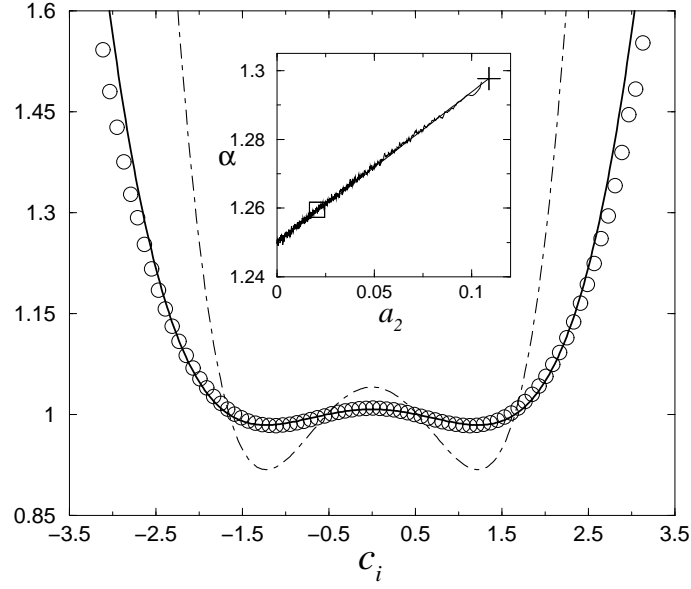


FIG. 8: Plot of  $\tilde{f}(c_i)/\mathcal{M}(c_i)$  as a function of  $c_i$ , at the particular time  $t_{1/2}$  where the density is exactly half the initial one, with the same initial distribution as in Fig. 7 [the circles (DSMC measure) thus show the same distribution as the circles of Fig. 7]. The thick curve shows  $1 + a_2(t_{1/2})S_2$  with  $a_2(t_{1/2})$  measured from its definition (54). The dashed curve is the Sonine prediction in the scaling regime (i.e. the thick curve of Fig. 7). Inset:  $\alpha$  as a function of  $a_2$  (see main text). The DSMC measure is compared to the prediction (B10) shown by the straight line ending at the point –indicated by a cross– of coordinates (0.109, 1.297) as predicted by Eqs. (58) and (59). The square located at (0.0207, 1.2595) corresponds to the numerical measure of  $\alpha$  and  $a_2$  made at time  $t_{1/2}$  for which the velocity distribution is displayed in the main graph.

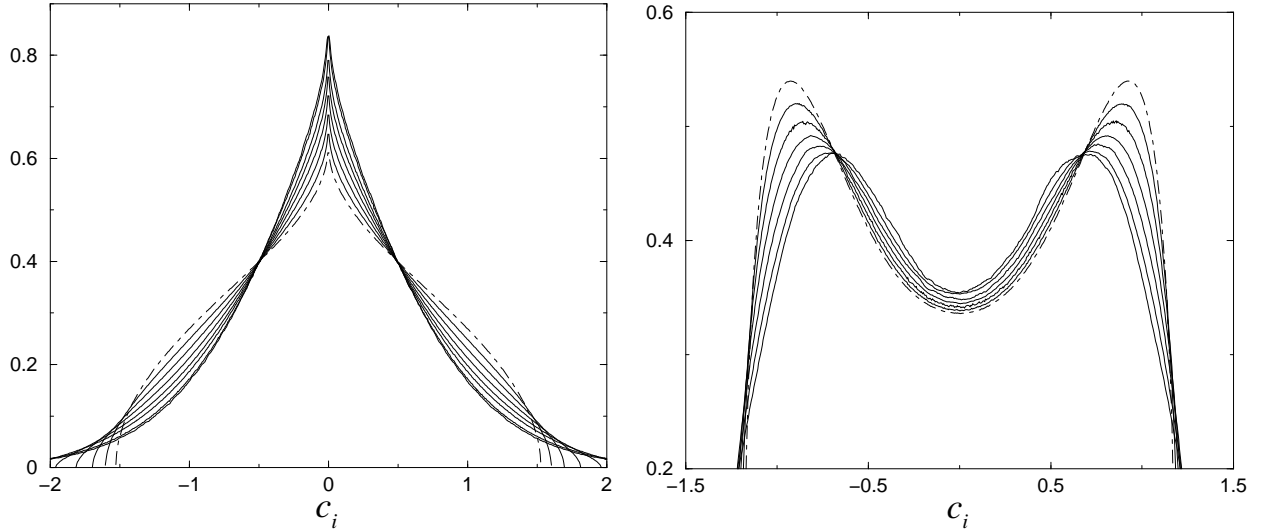


FIG. 9: Plots of  $\tilde{f}_1(c_i)$  as a function of  $c_i$  at different times. The left graph corresponds to an initial velocity distribution with  $\mu = -3/2$  while  $\mu = 3$  for the right graph. On both graphs, the initial distribution is shown by the dashed curve, whereas the thick curves display the asymptotic distributions approached in the scaling regime.